Mon. Not. R. astr. Soc. (1988) **235,** 827–856

The Durham/Anglo-Australian Telescope faint galaxy redshift survey

T. J. Broadhurst, R. S. Ellis and T. Shanks *Physics Department, University of Durham, South Road, Durham DH1 3LE*

Accepted 1988 August 1. Received 1988 July 14; in original form 1988 April 18

Summary. Using the fibre optic coupler at the Anglo-Australian Observatory, we have completed a new faint galaxy redshift survey. Intermediate dispersion spectra with resolution ~4 Å have been gathered for over 200 field galaxies selected in apparent magnitude slices between $20.0 < b_J < 21.5$ mag in five high-latitude fields. Redshift completeness is 85 per cent and the mean redshift agrees well from field to field.

Although the slope of the number–magnitude–count relation is considerably steeper than no-evolution predictions at $b_J \sim 21$ mag, the redshift range observed is similar to that expected in a non-evolving population. If our fields are representative, luminosity evolution can only be occurring in low-luminosity galaxies over the past 5 Gyr ($H_0 = 50$ km s^{-1} Mpc^{-1} used here and throughout the paper). However, the faint spectra reveal strong evidence for enhanced star formation in a large proportion of the galaxies beyond $z \sim 0.1$, which cannot be explained in terms of colour or aperture selection-effects. We suggest that it is these star-forming galaxies which represent the excess in the galaxy counts, at least at $b_J \sim 21$–22 mag.

The colour and absorption-line features in these galaxies can only be reproduced with models incorporating strong short-lived bursts of star formation which temporarily brighten these otherwise low-luminosity systems. We outline a physical model accounting for the observations whereby only galaxies at the faint end of the luminosity function evolve via discrete short-lived bursts of star formation.

1 Introduction

It has long been realized that studies of faint galaxies contain information on their evolution and role in determining cosmological parameters. Whilst much work has concentrated on studies of galaxies in distant clusters, only statistically complete samples of representative *field* galaxies can avoid complex selection effects associated with studies of rare subsets of the galaxy population.

Over the last 10 years it has become clear from automated photometric analyses of photographic prime focus plates (Kron 1978; Peterson *et al.* 1979; Tyson & Jarvis 1979; Shanks *et*

al. 1984) that the observed slope of the number–magnitude relation, $N(m)$, is steeper than expected. Detailed modelling of the counts and colour distributions of faint galaxies led to the conclusion that galaxies were more luminous and bluer in the recent past by virtue of an enhanced star-formation rate (see reviews by Ellis 1982; Kron 1982; Koo 1986a).

However, as Kron (1982) pointed out, it is premature to attribute the observed excess of galaxies fainter than $B \sim 21$ to luminosity evolution over the past few Gyr, without direct evidence of the mean redshift at that magnitude. The number of low-luminosity galaxies per unit volume remains quite uncertain in local redshift surveys (*cf.* Ellis 1987a) yet their fraction of the total population of galaxies *increases* at fainter apparent magnitudes since they suffer minimal redshift dimming. Might the excess of faint galaxies be due to a local population of dwarf galaxies omitted in the count models? Only the redshift distribution of a complete sample of faint galaxies can resolve this question.

It is extremely difficult to determine galaxy redshifts from photometric data alone. Whilst there have been attempts to use multicolour data to determine approximate redshifts (*cf.* Koo 1985; Loh & Spillar 1986), the technique relies on a complete knowledge or modelling of galaxy spectra-energy distributions, their time-dependence and range. Furthermore, since the count slope is steep in the blue, those selected at that wavelength are the most important to study yet the hardest to obtain photometric redshifts for, since their spectral energy distributions are generally flat. Also, should a hitherto unknown class of object be present at faint magnitudes, it would probably be difficult to identify this from colour analyses alone. Fortunately, progress in multiple object instrumentation such as fibre optic couplers and multislit aperture plates (Ellis & Parry 1987) at last makes it practical to gather genuine spectra at sufficiently faint magnitudes to address the origin of the steep number–magnitude slope.

This paper presents the first results from a deep spectroscopic survey of ~ 200 galaxies measured using the fibre optic coupler, FOCAP, at the Anglo–Australian Telescope. We discuss the strategy of our survey and observing/data reduction techniques in Section 2. The redshift distribution observed is compared with model predictions in Section 3 and we test for luminosity evolution and a faint end extension of the galaxy luminosity function in Sections 4 and 5. As neither of the two hypotheses appears to fit the observations, in Section 6 we compare the faint galaxy spectra with those obtained in a magnitude-limited survey of bright galaxies. Evidence for strong star-formation activity is found in *some* of the galaxies. In Section 7 we discuss the implications of this result and present a new model of galaxy evolution, consistent with the count and redshift distributions at faint limits.

2 The faint galaxy survey

2.1 STRATEGY

When our survey was conceived, its goal was to resolve the question posed by Kron (1982) – does the excess of faint galaxies form a high redshift tail to the no-evolution distribution (such as would be expected if the excess were due to luminosity evolution), or is there a low redshift tail of low-luminosity galaxies?

The essential requirement of the survey was that a redshift distribution should be obtained for a large statistically complete magnitude-limited sample of galaxies at a limit where the galaxy-count slope departs significantly from the best estimate no-evolution prediction. Since the departure from the no-evolution slope is greatest in the photographic blue passband, galaxies were selected at this wavelength. For efficient observing with multiple-object instrumenation, it is more convenient to select objects within a magnitude-limited *slice* rather than observe all galaxies brighter than some limit. Practicalities of observing time and instru-

mentation led us to adopt a magnitude range of $20 < b_J < 21.5$ (b_J = Kodak IIIa–J plus Schott GG385) as a reasonable compromise between the desire to go as faint as possible yet gather a sample of at least 100 galaxies. At $b_J = 21.5$, a satisfactory spectrum can be obtained on the AAT at 4 Å resolution using the Image Photon Counting System (IPCS) in under a night's exposure, yet at this limit even non-evolving models predict that we should observe galaxies as distant as $z \sim 0.4$.

The field centres for the survey were chosen randomly from a variety of high-latitude deep areas available to the Durham group in its various photometric programmes, according to the scheduling of the spectroscopic telescope time. In each of five fields, galaxies were selected on the basis of apparent magnitude and non-stellar profile from measuring machine scans of the photographic material. Our procedures for galaxy photometry and star/galaxy separation have been discussed at length in earlier papers (*cf.* Peterson *et al.* 1979; Shanks *et al.* 1984), but we briefly summarize the techniques here.

For three fields, prime focus b_J AAT plates were available and photometry was possible to an isophote of 1–2 per cent of the night-sky brightness, typically a surface brightness of $\mu = 26$ b_J mag arcsec^{-2}. Galaxies in these fields were selected from 10–20 × 20 arcmin areas in the magnitude range $20.5 < b_J < 21.5$. Two additional Schmidt fields were photometered in the slightly brighter range $20.0 < b_J < 21.0$. Although this isophote was somewhat brighter, 25 b_J mag arcsec^{-2}, detailed work (Shanks *et al.*) has shown the magnitudes at these limits are not seriously affected by small changes in the limiting isophote. In each field, the photometric calibration is based on CCD photometry of stars and galaxies taken under good conditions.

Star/galaxy separation was initially based on algorithms defined in the earlier papers but each spectroscopic target was visually checked and a small number of misclassifications, merged objects and plate defects were rejected. Finally, since our multiple-object technique cannot accept object pairs closer than 18 arcsec, in a small number of close pairs, only one object was chosen. These manual deletions to the otherwise machine-generated catalogue affected at most 10 per cent of the sample. The precise field areas and sample sizes are given in Table 1.

Altogether a total of 230 galaxies were chosen in the magnitude range $20 < b_J < 21.5$. The sampling rates vary from field to field due to the number available in the required magnitude range. The catalogue of spectroscopic targets is a strictly apparent magnitude-limited sample except for two details. We chose not to determine how many (if any) of the objects with stellar profiles might be compact galaxies. To do this would have doubled the spectroscopic time required since *all* stellar objects would have to be surveyed as well; furthermore, from the spectroscopic survey of Morton, Krug & Tritton (1985) to $B = 20$, there seems no indication that an extragalactic population is hiding in the stellar component (apart from QSOs).

These spectroscopic samples are, of course, insufficient in size and do not penetrate to faint enough limiting magnitudes to reliably define count *slopes*. We must therefore assume that

Table 1. Observations.

R.A.	Dec	Field	Magnitude Limits (b_J)	Field Size	Exposure Time	Sampling Rate	Completeness	$\bar{z}$
005436	-275450	SGP	20.5–21.5	22.8′ × 9.5′	29,300s	1/1	59/70	.225
015930	-495959	197	20.5–21.5	20.0′ × 20.0′	25,800s	1/1	31/38	.249
220303	-185442	MT	20.5–21.35	20.0′ × 20.0′	13,500s	1/2	30/35	.235
205556	-252554	529	20.0–21.0	24.6′ × 11.2′	22,500s	1/3	35/41	.209
035458	-310237	419	20.0–21.0	22.4′ × 22.4′	16,000s	1/3	32/36	.193

these fields are indeed representative of the larger areas scanned in the photometric surveys. This seems reasonable given the good agreement between observers on the slope of the counts from different areas, as well as the fact that the absolute numbers within each spectroscopic-survey area are always close to those predicted on the basis of the large photometric-survey area. Note also that two of the fields from which the spectroscopic samples are drawn were historic ones in establishing the steep count slope (Peterson *et al.* 1979; Shanks *et al.* 1984).

2.2 DATA ACQUISITION

Spectroscopic observations were made using the FOCAP fibre-optic multi-object coupler at the AAT (see Gray 1986; Ellis & Parry 1987 for technical details) during six clear nights out of 10 allocated to the project during 1985 August and November and 1986 August.

At the AAT Cassegrain focus, 50 fibres of diameter 2.67 arcsec were fed to the RGO spectrograph equipped with a 66 Å mm^{-1} grating and the IPCS as a detector. For three of a total of five runs, a further 50 fibres were also fed to the low-dispersion Faint Object Red Spectrograph (FORS), a fixed-format high-throughput collimatorless spectrograph with a GEC CCD detector inside an evacuated Schmidt camera. In each case six of the 50 fibres were dedicated to recording sky spectra; the sky positions were determined from the absence of objects to $b_J = 24.5$ on the prime focus plates and to $b_J = 22$ on the Schmidt plates.

The IPCS data cover the wavelength range $\lambda\lambda$3850–6050 Å at 4 Å resolution and the FORS data $\lambda\lambda$5000–10000 Å at 15 Å resolution. The bulk of the redshifts were measured using the IPCS data where the targets were strictly controlled according to the magnitude limit. The FORS data are of such low resolution that only strong features can be seen, and for that reason the FORS galaxy samples were not so carefully selected. To begin with, the FORS samples were simply a different random subset of the b_J-selected catalogue, but as IPCS redshifts became available through on-line data reduction, we transferred some of the successful IPCS targets to FORS for confirmatory exposures.

The wavelength range used for the IPCS observations ($\lambda\lambda$3850–6050 Å) samples the distinctive spectral features, [O II] 3727 Å and Ca II *H* and *K* 3968, 3933 Å over the interval $0 < z < 0.6$, ideal for examining most models likely to explain the number counts. Although FORS did not generate a large redshift list, the additional wavelength coverage does allow us to constrain the possibility that a number of high-redshift ($z > 0.6$) galaxies may be present in the samples (see later).

Long exposures of 15000–30000 s were made on each field according to the magnitude limit and observing conditions (see Table 1). Blank sky offset and calibration lamp exposures were taken at intervals of 3000 s, the former to measure hour-angle variations in the fibre–fibre response. Spectrophotometric standards were taken through individual fibres and relative spectrophotometry is discussed in Section 6.

2.3 DATA REDUCTION

Within the magnitude range of the survey the typical ratio of object count/sky count is 0.1–0.25 and hence careful sky-subtraction is essential. The method of sky-subtraction and fibre-transmission calibration for this set-up is well-established (see Ellis *et al.* 1984; Sharples *et al.* 1985; Ellis & Parry 1987). In this analysis we adhered to this practice but included run weighting, following the method described by Robertson (1986). This allows for variations in object/sky count resulting from changes in observing conditions, zenith distance and field guiding accuracy.

An important question to address is the precision to which sky-subtraction can be achieved with fibre optic couplers. We refer the reader to the review of Ellis & Parry (1987) for a full

discussion, but summarize the performance achieved in Fig. 1. The sky spectrum is recorded using six of the fibres spaced along the entrance slit of the spectrograph. The combined sky spectrum for each field run when subtracted from the individual sky fibres thus gives an indication of the sky-subtraction precision achieved. The nightly rms residual, averaged over the spectrum, is only 1.2 per cent of sky and only marginally above the photon noise expectation. There is no trend in the sky residual with fibre number, an observation of crucial importance for the measurement of spectral features and equivalent widths.

As discussed by Ellis & Parry, one of the limitations of fibres with FORS arises from the fact that the sky spectrum is highly structured, thus a 1 per cent sky-subtraction precision is still inadequate for absorption-line work when the features overlap the night sky OH emission bands. Together with the lower spectral resolution and slight undersampling, this explains the poor success rate of red FORS data.

Once sky-subtracted and flux-calibrated, redshifts were measured by line-fitting techniques for the emission-line spectra, and via cross-correlation with co-added nearby the intermediate redshift cluster galaxy templates for the absorption-line cases. The redshift precision in each case is typically ~ 100 km s^{-1} or $\delta z = 10^{-3}$. A very high proportion of galaxies revealed [O II] 3727 Å which occasionally was the only emission feature visible. Fortunately, in nearly all cases, the single line ID can be verified from Balmer absorption-line measurements. A sample of the reduced spectra is shown in Fig. 2.

2.4 COMPLETENESS

Completeness is clearly an important factor in ensuring the redshift distribution, $N(z)$, is representative of the magnitude-limited sample. First, we note that only two of our fields are

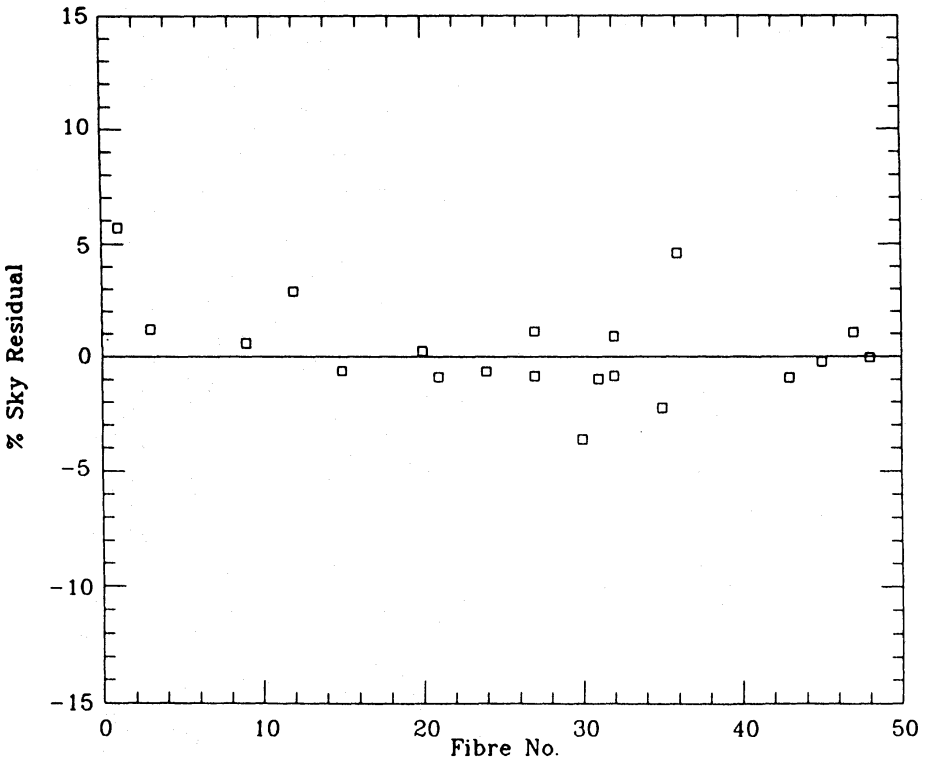

Figure 1. An estimate of sky-subtraction quality using fibres at faint magnitudes: the residual sky after sky-subtraction for sky-dedicated fibres as a percentage of the total sky recorded per fibre per night ($\sim 12\,000$ s integration), plotted against fibre number.

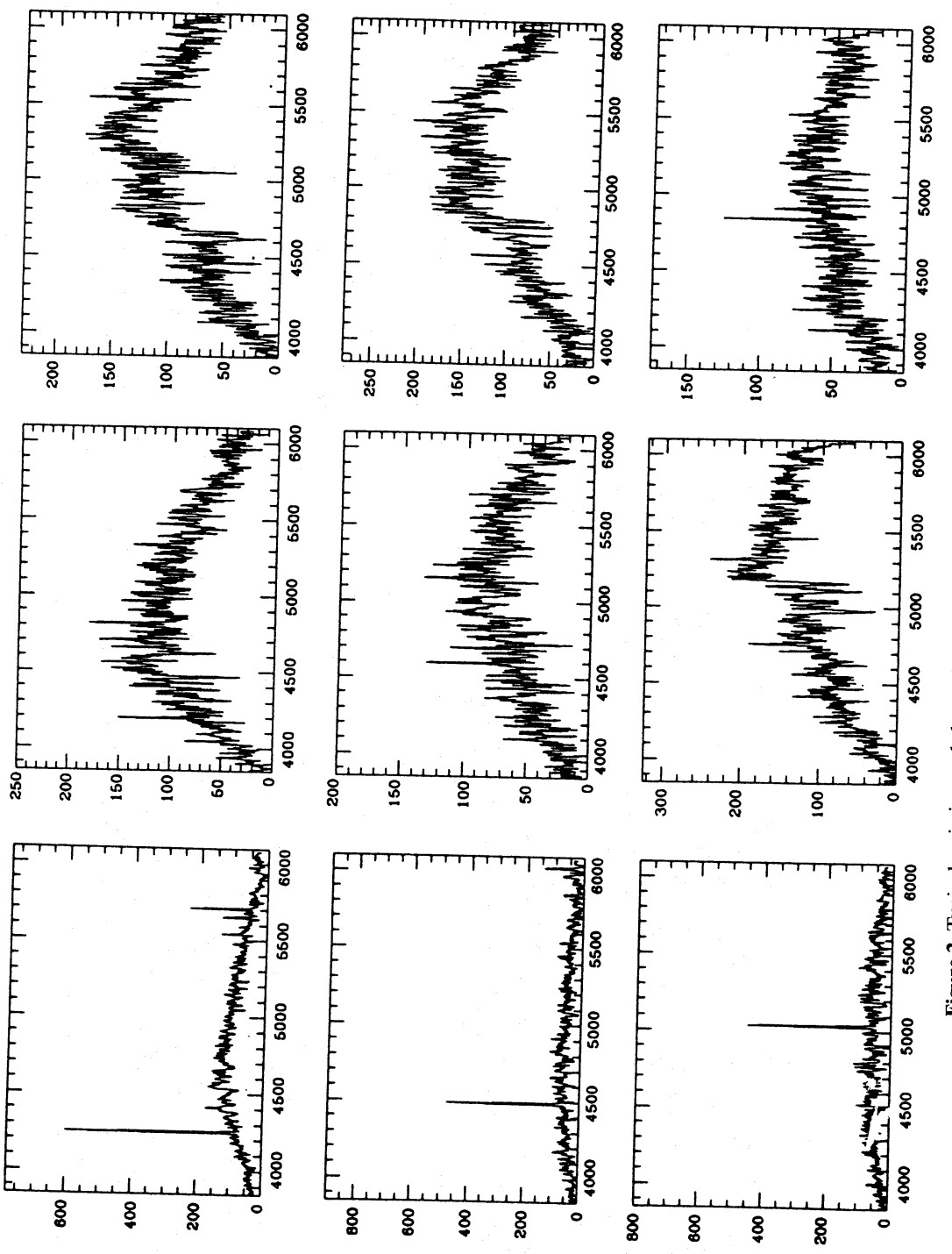

Figure 2. Typical emission and absorption-line spectra from galaxies with $b_J \sim 21$.

fully sampled, i.e. all galaxies in the area were studied (see Table 1). However, for the other three fields, objects were selected purely at random within the magnitude limits chosen, and so we may assume these fields are also representative of complete samples.

The completeness in redshift achieved with the IPCS data is very high for all fields, ranging from 82 to 89 per cent. Of a total of 230 spectra acquired with the IPCS, redshifts were successfully secured for 187, note that a few stellar spectra and spectra recorded through defective fibres have been removed, leaving a total of 220 galaxies. The objects for which a redshift could *not* be assigned are those for which the observed photon count is demonstrably smaller mainly as a result of the object position on the detector, which suffers from vignetting of up to 40 per cent at the slit edge. Consequently, there is only a very weak dependence of completeness and apparent magnitude (Table 2).

As remarked above, the available redshift window for the frequently seen [O II] 3727 Å is $0 < z < 0.6$. However, the redshifts observed all lie below $z = 0.47$. Although our completeness varies from field to field, the mean redshift and range in redshifts are very similar. It is therefore unlikely that the objects without redshift lie beyond the observable redshift window. The spectral coverage of FORS complements that of the IPCS in this respect and we are thus able to extend the search for emission-line objects to $z < 1.0$; however, no high redshift galaxies were found (although some confirmatory [O III] and Hα emission in lower redshift galaxies were noted). In fact, the redshift range derived from the sparse FORS data (30 galaxies) is very similar to that seen in the IPCS data. We thus conclude that the present level of completeness is sufficient for defining the redshift distribution of field galaxies in the magnitude range observed.

2.5 THE CATALOGUE

The final redshift catalogue is listed in Table 3. For each field we list the galaxy ID regardless of whether a redshift was eventually determined; this hopefully may encourage other observers to complete the survey! The astrometric position in 1950.0 coordinates is accurate to < 0.5 arcsec precision rms. In the case of the emission and/or absorption redshift, these are uncorrected for any local motions. Column 7 lists the cross-correlation coefficient, r (Tonry & Davis 1979). The final column lists the rest-frame equivalent width, W_λ, for the [O II] 3727 Å emission line (see discussion in Section 6.1). Those objects determined to be stars are included in the catalogue for completeness but are eliminated from the analysis henceforth.

3 No-evolution predictions

In this section we attempt to reconcile the redshift distribution, $N(z)$, observed with the simplest possible model, namely that galaxies share the same properties as those measured in our nearby redshift survey (Peterson *et al.* 1986). Whilst the no-evolution model is already in difficulty in explaining the number-magnitude-colour distributions, we will use the no-evolution $N(z)$ as a basis for the more detailed modelling described in the next section.

Table 2. Magnitude–redshift data.

m_{b_j} limits	No. of fields	Completeness	$\bar{z}$
20.0-20.5	2	29/32	0.188
20.5-21.0	5	97/108	0.225±0.015
21.0-21.5	3	61/80	0.235

Table 3. Catalogue.

	RA	Dec.	m_{b_J}	z_{em}	z_{abs}	r	W_λ (Å)
	SGP	Field					
1	005427.32	-275528.9	21.48	.3691	.3695	2.57	31
2	005438.83	-275342.4	21.08	.2152	.2159	4.66	19
3	005435.77	-275543.7	21.41	.3897			16
4	005349.41	-275140.0	20.97	.1120			58
5	005428.35	-275106.8	20.83	.2488	.2493	4.43	25
6	005438.06	-275608.4	20.86	.3196	.3203	2.49	30
7	005516.19	-274944.9	21.04		.2751	6.42	0
8	005520.72	-275238.6	21.47		.2750	3.39	3
9	005501.45	-275202.1	21.16				
10	005508.94	-275231.4	20.66		.1610	3.18	2
11	005517.51	-274935.8	21.09	.1577	.1581	3.78	84
12	005524.95	-275441.1	21.42	.1168			47
13	005518.33	-275622.3	20.59	.2140	.2146	3.53	48
14	005417.94	-275244.5	21.01				
15	005423.28	-275613.8	21.40	.2254	.2261	2.15	28
16	005410.15	-275920.8	21.12	.2030	.2040		41
17	005408.64	-275549.6	21.25	.3191	.3187	2.39	27
18	005418.73	-275742.4	21.02	.4054	.4060	2.92	11
19	005419.05	-275149.4	20.72	.1658	.1665	2.94	22
20	005412.29	-275615.4	21.26	.3489	.3490	3.91	14
21	005406.73	-274939.6	20.85	.2132	.2137	3.66	17
22	005353.07	-275912.0	20.65	.1679	.1684	3.40	24
23	005353.53	-275933.1	21.03	.1052	.1057	3.33	41
24	005347.74	-275804.8	21.48				
25	005357.36	-275453.6	20.61	.1150	.1156	3.53	23
26	005357.12	-275351.9	20.87	.1157			73
27	005457.86	-275902.5	21.39	.2755	.2762	2.92	15
28	005453.71	-275854.1	20.81		.2737	3.16	11
29	005440.41	-275616.0	21.31				
30	005444.88	-275418.2	21.13	.2155	.2165	3.41	33
31	005440.49	-275805.8	21.18	.2136	.2144	2.74	19
32	005526.93	-275753.3	21.44	.1247			71
33	005444.75	-275656.0	20.52	.2981	.2976	4.39	16
34	005426.17	-275233.8	20.78	.1604	.1608	3.05	16
35	005456.37	-275139.6	21.19	.1629			35
36	005506.49	-275313.6	20.91	.1607	.1615	3.18	32
37	005406.27	-275652.7	21.47	.1619			15
38	005412.76	-275646.5	20.94				
39	005348.76	-275933.4	20.54				
40	005357.52	-274959.1	21.35	.4442			76
41	005443.36	-275636.6	20.50		.1646	5.50	3
42	005355.88	-275319.2	21.28	.2117			30
43	005353.16	-275526.9	21.49	.3462	.3455	2.16	5
44	005346.94	-275039.1	21.45				

Table 3 – *continued*

	RA	Dec.	m_{b_J}	z_{cm}	z_{abs}	r	W_λ (Å)
45	005518.155	-275237.99	20.50		.2090	2.23	0
46	005417.560	-275307.35	20.57	.2156	.2155	3.91	6
47	005440.920	-275836.89	20.60	.1620			55
48	005519.276	-275628.24	20.66				
49	005450.541	-275912.10	20.70	.2757	.2756	3.06	24
50	005356.059	-275558.63	20.80		.1793	4.20	0
51	005349.354	-275745.92	20.82		.2119	4.55	2
52	005505.948	-274929.14	20.85		.2123	4.58	0
53	005454.412	-275459.61	20.90	.1171	.1173	1.92	47
54	005509.216	-275022.41	20.94		.1647	1.91	15
55	005514.116	-275540.69	20.98	.0409			100
56	005358.479	-275300.42	21.02		.2749	3.14	4
57	005451.546	-275625.89	21.04	.1136			98
58	005418.723	-275006.78	21.08	.3194	.3205	3.50	9
59	005444.169	-275116.87	21.11	.1198	.1217	2.43	13
60	005452.453	-274925.86	21.13	.3339	.3341	2.23	18
61	005348.905	-275559.35	21.17	.2359			49
62	005521.073	-275447.02	21.22				
63	005349.809	-275616.70	21.26		.2776	2.51	0
64	005455.129	-275524.70	21.29				
65	005500.627	-275033.81	21.33	.2359			43
66	005415.314	-275006.02	21.39	.3329	.3339	2.28	30
67	005413.846	-275537.61	21.40	.3468	.3473	3.18	23
67	005448.863	-274938.72	21.42				
69	005345.582	-275930.10	21.45				
70	005419.610	-275331.01	21.47		.2114	2.90	6
71	005519.228	-275735.87	21.48	.1628			25
	197	Field					
1	020013.48	-500532.6	21.03	.1730	.1733	2.83	33
2	015942.60	-500227.6	21.48				
3	020000.16	-500519.6	20.81	.3518	.3518	2.80	20
4	015957.29	-500212.0	21.08	.1439	.1440	3.36	19
5	020001.53	-500545.6	21.33				
6	015947.76	-500210.3	21.45	.1010			15
7	015935.40	-500509.2	21.04	.0891			39
8	015929.31	-500536.2	20.73	.3509			31
9	020025.26	-500255.5	20.98		.3071	4.45	0
10	020037.34	-500428.2	20.74	.1014			28
11	020033.78	-500907.1	21.34	.2171	.2169	2.30	24
12	020050.33	-500503.7	21.15	.2082			46
13	020029.85	-500259.7	20.90	.3065	.3064	2.80	10
14	020038.21	-500249.9	20.59	.4736	.4738	3.46	10
15	020041.48	-500812.5	21.23		.2168	3.23	0
16	020027.16	-500614.2	20.82	.3856	.3864	3.42	15
17	020034.99	-500152.9	20.93	.3755	.3756	3.38	15

Table 3 – *continued*

	RA	Dec.	m_{b_J}	z_{em}	z_{abs}	r	W_λ (Å)
18	020012.62	-495934.6	20.78	.2118	.2121	4.00	14
19	015953.04	-500847.1	21.37	.2074	.2080	3.04	54
20	020056.62	-500005.0	21.25	.1002			70
21	020005.16	-500632.7	20.95	.1013			33
22	020105.47	-495919.6	21.41	.3509			49
23	020020.14	-495927.8	21.28	.3089	.3095	2.62	8
24	020030.79	-495853.4	21.13				
25	020102.24	-495453.4	20.61	.3069	.3070	4.40	13
26	015912.80	-500402.7	21.43				
27	015909.68	-495907.3	20.65	.1846	.1854	2.74	36
28	015908.59	-500251.8	21.19				
29	015918.54	-500527.3	21.48	.1961	.1961	2.10	26
30	015919.53	-495905.8	21.32	.3839	.3832	2.68	30
31	015923.49	-495903.3	20.90	.1838			37
32	020045.41	-495406.8	20.76	.2643	.2652	3.84	17
33	020029.66	-495105.5	21.22	.1939	.1941	2.97	13
34	015950.13	-495207.7	21.34		.3847	2.67	0
35	020004.07	-495450.8	20.62	.2652	.2658	3.06	28
36	020008.18	-495152.1	21.36				
37	015941.36	-495334.8	21.21				
38	015912.50	-495406.9	20.68		.2251	2.20	0
39	020014.56	-495407.5	21.39				
	MT	**Field**					
1	220229.50	-185501.92	20.50	.3465	.3464	3.27	11
2	220237.69	-185136.06	20.52	.1900	.1898	3.32	15
3	220336.63	-184127.90	20.54	.2121	.2127	3.04	32
4	220336.25	-184642.29	20.56	.1604			32
5	220237.10	-190504.55	20.58		.1490		0
6	220320.84	-184707.09	20.65		.2411	3.97	8
7	220328.41	-190650.77	20.66		.1351	5.15	0
8	220329.60	-190603.66	20.67		.1343	4.01	0
9	220356.29	-190350.90	20.68		.3094	4.14	0
10	220242.69	-190014.35	20.73				
11	220251.06	-185350.54	20.75		.2372	5.70	3
12	220309.27	-190630.20	20.77	.3280	.3285	2.47	28
13	220233.18	-185715.37	20.81	.2376	.2379	4.13	15
14	220232.63	-184651.72	20.84		.2631	2.65	22
15	220242.60	-185744.35	20.86	.2099	.2109	3.15	19
16	220243.85	-185314.36	20.87				
17	220207.86	-184911.64	20.89	.2359	.2362	2.98	55
18	220342.20	-184845.29	20.92	.2384	.2389	2.81	35
19	220208.70	-185452.20	20.95	.2295	.2299	2.85	14
20	220302.87	-190651.27	20.95	.1537			14
21	220204.78	-184301.39	20.96				
22	220315.94	-184700.08	21.01	.2724	.2735	3.14	23

Table 3 – *continued*

	RA	Dec.	m_{b_J}	z_{cm}	z_{abs}	r	W_λ (Å)
23	220236.06	-184107.06	21.04	.1861			24
24	220247.82	-190250.07	21.05	.3334			12
25	220231.04	-185340.74	21.07				
26	220400.99	-184554.72	21.09				
27	220332.23	-190325.63	21.12	.1520	.1521	2.62	10
28	220249.97	-184552.76	21.14	.3623	.3621	2.91	18
29	220215.92	-184733.05	21.16	.2840			22
30	220223.59	-184848.81	21.21	.1860			25
31	220235.22	-190712.88	21.22				
32	220324.56	-185406.40	21.22	.1745	.1749	2.76	40
33	220312.61	-185831.80	21.23				
34	220344.61	-184427.73	21.26				
35	220231.39	-190523.19	21.28	.2991	.2996	2.99	26
36	220335.91	-185504.55	21.28	.4235			50
37	220341.03	-184244.53	21.30	.1751			15
38	220253.35	-185412.57	21.34	.0968			52
39	220312.68	-185159.60	21.36				
40	220208.39	-185224.81	21.38				
41	220313.19	-185332.52	21.41				
42	220223.63	-184621.97	21.44				
43	220400.52	-185307.76	21.47				
44	220230.15	-185845.47	21.49	.1459	.1463	2.36	46
	419	Field					
1	035544.54	-311132.6	20.42	.1661	.1663	2.85	17
2	035538.54	-310907.5	20.67		.1746	3.23	18
3	035527.93	-311026.9	20.88	.1076			10
4	035534.46	-311246.3	20.26	.2245			25
5	035515.32	-311147.7	20.01	.2993	.2991	2.74	10
6	035546.82	-311233.1	20.06	.1398	.1405	3.09	49
7	035515.35	-310300.9	20.28	.3600			10
8	035544.35	-310410.1	20.70	.1739	.1745	3.00	20
9	035515.70	-310207.8	20.89	.2200	.2199	4.75	23
10	035519.87	-310424.6	20.99	.1417			33
11	035548.03	-305736.6	20.91	.2424	.2431	3.05	11
12	035507.95	-310300.3	20.94	.1666	.1671	4.01	37
13	035531.05	-310340.5	20.93				
14	035547.09	-310414.2	20.66		.1735	3.05	0
15	035516.60	-310116.5	20.86	.3258	.3263	2.73	10
16	035511.20	-310112.7	20.77		.2073	3.44	11
17	035413.74	-305630.8	20.18				
18	035405.66	-305442.5	20.13	.1986	.1988	4.88	7
19	035452.54	-305514.5	20.11	.0934	.0942	3.11	26
20	035425.73	-311205.6	20.38	.1764	.1771	4.53	4
21	035405.57	-305255.1	20.81	.1414			51
22	035416.73	-305523.1	20.23		.2333	4.63	0

Table 3 – *continued*

	RA	Dec.	m_{b_J}	z_{cm}	z_{abs}	r	W_λ (Å)
23	035425.76	-310637.8	20.36	.0611			26
24	035444.68	-305328.0	20.03	.2542	.2541	4.56	3
25	035450.61	-305344.1	20.99				
26	035420.00	-305518.3	20.99	.2532	.2535	3.87	29
27	035450.61	-305344.1	20.99	.2036	.2047	2.84	65
28	035412.31	-311307.1	20.16	.1250	.1252	4.23	10
29	035447.21	-310935.6	20.73				
30	035434.30	-310848.3	20.14	.2318	.2327	3.86	34
31	035413.35	-311243.5	20.57	.1936	.1941	5.21	25
32	035454.78	-310518.0	20.52		.2992	5.10	0
33	035428.43	-311109.7	20.88	.2020	.2020	2.85	33
34	035453.45	-311201.5	20.99				
35	035506.18	-305813.2	20.62	.2649	.2657	2.60	52
36	035448.88	-305741.5	20.53	.2329	.2329	3.27	8
37	035453.43	-310225.9	20.49				
38	035501.16	-310025.2	20.46		.2074	3.85	1
	529	Field					
1	205650.66	-252453.9	20.88	.1988	.1993	2.90	59
2	205639.14	-252335.5	20.81		.1984	2.46	
3	205610.44	-252115.1	20.63	.1086			40
4	205626.45	-252236.0	20.69		.3009	4.91	2
5	205609.03	-252029.4	20.00	.1874	.1885	4.16	25
6	205649.80	-252342.3	20.89		.2997	3.17	0
7	205635.31	-253101.7	20.83	.1980	.1999	2.79	24
8	205634.67	-253121.6	20.94	.1978	.1988	2.95	22
9	205556.95	-252716.4	20.73	.1718	.1721	3.81	11
10	205543.09	-252713.4	20.31		.1790	3.10	9
11	205535.16	-252827.8	20.04		.1649	4.97	2
12	205556.14	-253113.8	20.04	.1358	.1360	3.69	42
13	205514.91	-252344.3	20.94	.4357			16
14	205517.22	-253107.6	20.10		.1693	3.40	0
15	205615.02	-252638.3	20.94				
16	205623.78	-252605.1	20.27				
17	205552.48	-252310.6	20.69		.1855	1.82	2
18	205553.45	-252530.5	20.67	.3004	.3010	2.55	23
19	205630.83	-252728.1	20.63	.2901	.2910	5.47	5
20	205604.45	-252452.1	20.46				
21	205626.06	-252739.2	20.42	.1862	.1865	3.51	8
22	205633.42	-252848.7	20.44		.2029	2.97	9
23	205610.80	-252151.9	20.06	.3200	.3197	3.71	13
24	205545.94	-252231.2	20.54		.3170		0
25	205544.69	-252208.4	20.56	.2040	.2047	3.27	51
26	205555.59	-252135.6	20.98				
27	205643.05	-252737.4	20.92				

Table 3 – *continued*

	RA	Dec.	m_{b_J}	z_{em}	z_{abs}	r	W_λ (Å)
28	205551.52	-252019.0	20.97				
29	205555.06	-252026.1	20.67	.1686			35
30	205504.63	-251911.5	20.66				
31	205517.39	-251727.1	20.37		.1841	3.06	2
32	205520.16	-252001.1	20.10		.1865	5.15	20
33	205521.70	-251811.9	20.27	.1863			5
34	205648.84	-251839.5	20.24				
35	205643.52	-251657.1	20.60	.1984	.1990	3.05	11
36	205611.70	-251832.6	20.04	.0670			32
37	205613.66	-251324.8	20.48		.1335		2
38	205624.91	-251643.4	20.60	.3186	.3192	3.51	19
39	205602.59	-251858.8	20.81				
40	205625.19	-251411.7	20.48	.3173	.3176	2.85	29
41	205610.44	-251258.1	20.94	.1715			14
42	205517.56	-253030.0	20.23		.1707	3.37	
43	205520.84	-253104.5	20.60		.2011	3.67	11
44	205637.72	-252415.4	20.40	.0559			33

3.1 THE OBSERVED REDSHIFT DISTRIBUTION

The redshift distribution presented in Fig. 3(a) is co-added from all survey fields and weighted by the inverse ratio of the number of galaxies observed per field to the average of all fields, this ensures the resultant distribution is not biassed by the clustering of individual fields. This distribution is relatively smooth, as expected for a well-defined selection function based on a galaxy-luminosity function which is not discontinuous. However, the distribution within each field shows obvious clustering in redshift space and considerable variation in structure is apparent from field to field, see Fig. 3(b). The 3D clustering within the survey, its relevance to the fluctuations in the galaxy counts, and the growth of large-scale structure, will be discussed elsewhere (see Ellis 1987a for a preliminary discussion). Typical velocity errors on individual redshift measurements are very small at the resolution of this work and so do not affect the gross properties of the distribution considered here.

Table 1 shows the mean redshift for each field, note that fields with matched magnitude limits have similar means. This may be expected since, as is evident from the co-added distribution, the majority of objects are most readily sampled in a rather narrow redshift range which is symmetric about the mean, and so to first order the mean is not sensitive to fluctuations in the redshift distribution caused by galaxy clustering.

3.2 THE NO-EVOLUTION MODEL

The method of construction of a model for predicting faint galaxy distributions has been outlined by many authors (see reviews referenced in Section 1); here we discuss those properties of local field galaxies which the models require, and the sensitivity of the faint galaxy redshift distributions to uncertainties in these properties.

Our local galaxy properties are provided by the Durham/Anglo-Australian redshift survey (DARS) of 340 galaxies limited at $b_J \sim 17$ (Peterson *et al.* 1986). Morphological types, redshifts and apparent magnitudes are available for all survey objects, and optical-infrared colours (b_J–K) are also available for a sub-sample of ~ 200 galaxies from the infrared survey of Mobasher *et al.* (1986).

Foremost, the DARS provides a reliable estimate of the field-luminosity function (LF) and its variation with Hubble type or b_J–K colour. To estimate this, we divide the DARS survey into three type groupings (E/S0, Sa through Sbc, and Sc through Im), apply the k correction

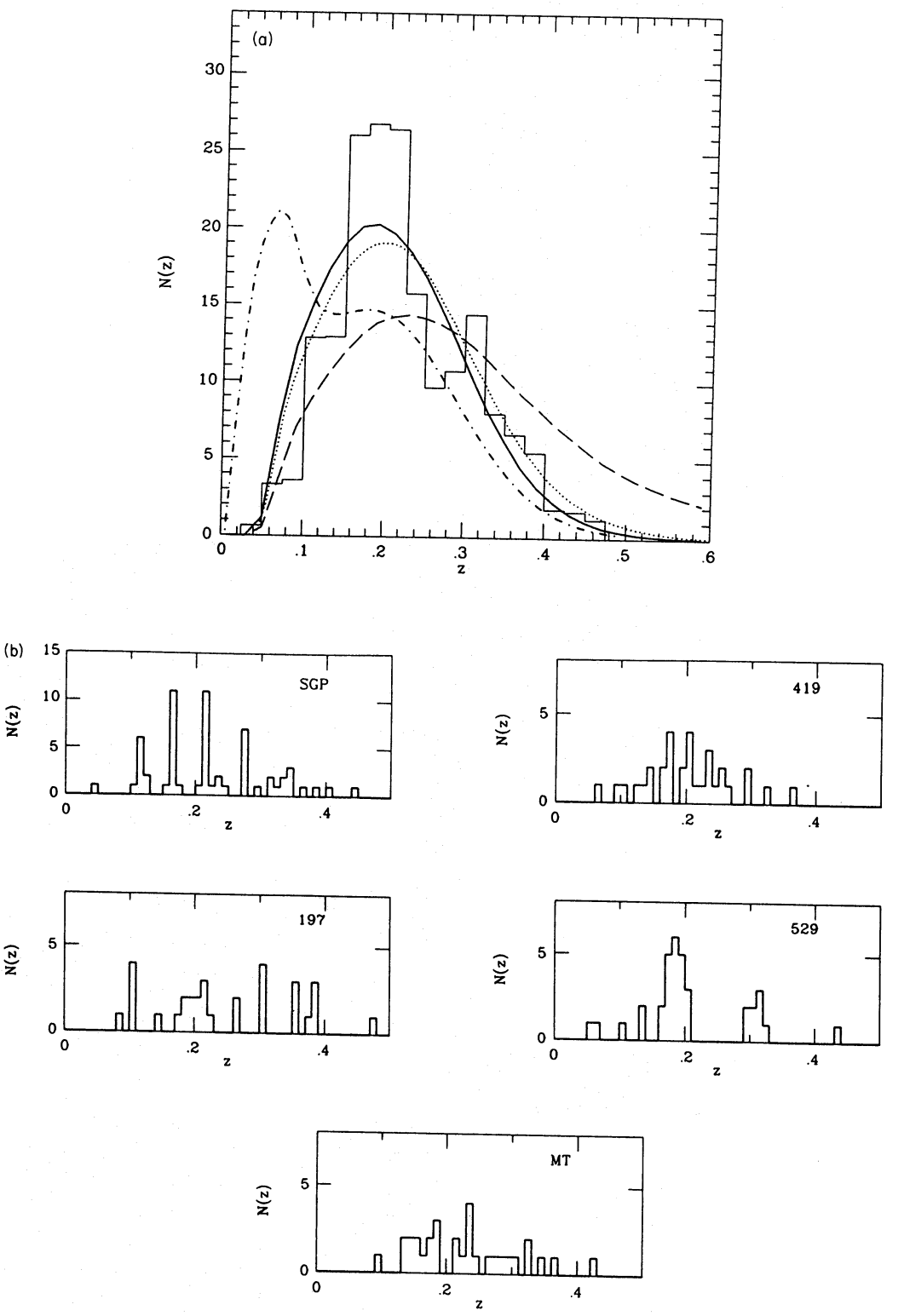

Figure 3. Redshift distribution (a) weighted co-addition of all fields, binned in $\delta z = 0.025$ bins, (b) for each individual field. The magnitude limits for the data are given in Table 1. Curves refer to model predictions as follows: solid – no evolution; dash – luminosity evolution adjusted to match the $N(m)$ slope; dot-dash – extension of the field-luminosity function adjusted to match the $N(m)$ slope; dotted – luminosity-dependent evolution of the form described in Section 5.2.

appropriate to each type, and hence determine the absolute magnitude distribution $N(M_{b_J})$ for each group. Following the technique described in Ellis (1982), we parameterize these distributions in terms of those expected for a Schechter (1976) function with a faint end slope, $\alpha = -1.25$, found for the entire survey (Bean 1983, Efstathiou *et al.* 1988) determining M^* from a minimum χ^2 fit. The trend towards fainter characteristic absolute magnitudes for later types is evident in the results summarized in Table 4.

We prefer this simple technique to a full Schechter function analysis for each type (as done by Efstathiou *et al.*) because the number of late-type galaxies, most important in predicting $N(b_J)$, is very small in the local surveys. Consequently the derived error bar on the faint end slope for this class is quite large. We return to uncertainties in the faint end of the LF and its effect on our conclusions in Section 5.

This technique is employed mainly to provide the trend of M^* with type which is most important in determining the average depth to which each type is seen and thus enabling a determination of the apparent change in mix with magnitude because of the k correction. In particular, the sum of the Schechter fits to the individual types will only accurately follow the fit for the entire population if the luminosity function of each type is well-described by the same Schechter function (which is only approximately true for the bluest galaxies).

The relative proportions of each galaxy type (mix) are found by adjusting the relative space densities so that a number-count model produces the observed fractions of each galaxy type in the DARS to the survey magnitude limit. The overall normalization remains quite uncertain, with the DARS volume density 40 per cent lower than most other LF estimates and that inferred from deeper photometry of 14 Schmidt fields (Stevenson *et al.* 1985). The origin of the DARS deficiency witnessed in each of the five well-calibrated distributed fields remains obscure. Fortunately, we are interested in the count slope in this paper; this, together with the form of faint $N(z)$ predictions is independent of the normalization, *provided the mix within the DARS is representative of that in samples of more typical number densities.* The mix determined from the DARS survey agrees well with that inferred from colour distributions in the deeper Schmidt photometry as well as that derived from the LFs split by b_J–K colour (see below).

For the k-corrections we note that the mean redshift of the new faint survey is typically ~ 0.25 and thus even at blue wavelengths, we do not penetrate the satellite ultraviolet region where genuine spectrophotometry is scarce and numerous systematic errors may be present in the data which is available. We use the k-corrections summarized by King & Ellis (1985) which rely primarily on the optical spectrophotometry of Wells (collated and tabulated by Pence 1976) for the various types.

Table 4. 'No-evolution parameters' ($H_0 = 50$).

Galaxy Type	$M^*_{b_J}$	#	Model Predictions
E/S0	−21.6	97	$\bar{z}(20.5 < b_J < 21) = 0.22$
Sab–Sbc	−21.15	117	$\gamma(20 < b_J < 24) = 0.32$
Sc–IM	−20.85	46	
B − K Limits	$M^*_{b_J}$	#	**Model Predictions**
> 3.65	−21.39	74	$\bar{z}(20.5 < b_J < 21) = 0.215$
2.9-3.65	−21.24	61	$\gamma(20 < b_J < 24) = 0.32$
< 2.9	−20.52	32	

3.3 MODEL PREDICTIONS

Observations of $N(b_J)$ by numerous authors have shown that whilst sizeable fluctuations in absolute numbers are seen from field to field, the differential counts are well-fitted by a single-valued slope for magnitudes fainter than $b_J = 20$. The slope determined for the magnitude range $20 < b_J < 23$ is $\gamma = d\log N/dm = 0.43 \pm 0.02$ (*cf.* King & Ellis 1985) and recent CCD photometry (Tyson 1987; Metcalfe *et al.* 1987) shows a similar slope extends to at least $b_J \sim 25$. The no-evolution model produces a continued flattening of the count slope with apparent magnitude due to redshift dimming, so that the predicted slope in the range $20 < b_J < 24$ has an average value of $\gamma = 0.32$, considerably lower than observed.

These no-evolution predictions are almost identical to those published by King & Ellis (1985) and Shanks *et al.* (1984), differing only in the precise parameters for the characteristic magnitudes of the local LF. As a check on the stability of our models we can redetermine the LF and mix in terms of b_J–K colours (Mobasher *et al.* 1987). Dividing this sample into three colour classes in b_J–K we determine the LF as described above. Table 4 shows the comparison of this method with the models based on morphological types. Again, very little difference is found in predictions of $N(b_J)$, $N(z)$, between these two completely different methods for parameterizing local galaxy properties. We thus conclude that we have constructed no-evolution models which represent the best available.

If we normalize the model at the brightest reliably determined count (corresponding to $b_J = 18$), then the predicted counts fall short of those observed by a factor of ~ 1.5 at $b_J = 21.5$, hence the earlier claims for luminosity evolution. Indeed if we limit the discussion to models which do *not* include evolutionary changes, extreme modifications of the local galaxy properties are required in order to produce the observed count slope which, as we show below, can be easily discriminated by observing $N(z)$ at faint magnitudes.

Fig. 3(a) shows the no-evolution prediction weighted to account for the different magnitude limits for each field. When comparing model redshift distributions with data, we normalize to the numbers of objects observed in the survey, both because of the uncertainty in space density referred to earlier and because the counts vary from field to field. We note there is good agreement between the predicted and observed redshift range.

This result is surprising because this model fails to account for the $N(m)$ count slope in the range $20 < b_J < 24$, and yet, as we show later the width of the field galaxy luminosity function implies that a spectroscopic survey to $b_J = 21.5$ contains valuable information on the origin of the steep count slope to much fainter magnitudes. It seems inconceivable, given the discussion above, that the no-evolution model could be adjusted to meet this challenge. We conclude that if additional objects are present at faint magnitudes, *they lie in the redshift range expected from those objects represented in the local field survey.*

To check that the survey is sufficiently large to provide a well-determined redshift distribution, we list in Table 2 the mean redshift, $\bar{z}$, for three successive magnitude intervals of width 0.5 mag. The trend found between $\bar{z}$ and the increasing apparent magnitude is well-behaved. Whilst the actual mean value at a given magnitude is clearly model dependent (see Sections 4 and 5), the derivative is less so and that observed is reasonably consistent with expectations. Furthermore, the error estimate, derived from the field-to-field scatter in $\bar{z}$, where there is a common Δm interval, gives a confident indication of the representative nature of the observed redshift distributions.

4 Tests for luminosity evolution

The conventional explanation for the steep slope of the blue number–magnitude counts is that at least some subset of the galaxies were more luminous in the past. This can be understood via

one of two pictures. Either main sequence brightening occurs in passively evolving systems, such as in Bruzual's (1983) *c*-models. Here a strong initial burst of star formation occurs at the formation redshift, z_f, and the detectability of such evolution depends critically on the value of z_f, becoming harder for early formation eras. Alternatively, star formation may be extended in duration but gradually declining with time (Bruzual's μ-models) and although the evolution seen has a similar origin, the amount expected depends on the precise form of the star-formation history, as well as the galactic age.

Previous quantitative conclusions for luminosity evolution have been derived from photometric data alone under various assumptions. Some authors (Shanks *et al.* 1984) made the assumption that *all* galaxies share the same evolutionary correction, which increases monotonically with redshift; this has the advantage that a correction is determined *empirically* from the counts, though the present range in galaxy colours suggests different galaxy types had different evolutionary histories. Other workers (Tinsley 1980; Koo 1981; Koo 1986b) have used models such as those of Bruzual (1983) to predict the past behaviour of all kinds of galaxies, attempting to reconcile both colours and counts for various cosmological models. This is probably more realistic but has the disadvantage that quantitative conclusions *rely* on the accuracy and appropriateness of the models.

Clearly, the precise way in which evolution is modelled affects any $N(z)$ prediction that we can compare with our survey. To keep this question straightforward, we examine how much evolution is needed to reproduce the steep count slope in the b_j passband and ask whether the $N(z)$ relation implied is consistent with the new observations. In Shanks *et al.*'s approximation where the evolution is shared by *all* types, this is straightforward, but in the framework explored by Koo and others we adopt the simplifying assumption that some subset (perhaps to be associated with the present day E/S0s) undergo luminosity and colour evolution according to Bruzual's μ- or *c*-models, with the remainder suffering no change at all.

Below, we compare the predictions of selected evolutionary models discussed in this section with the data presented above. Note that due allowance is made for the different magnitude limits of each field. We reach the following conclusions:

(i) *c*-models with strong initial bursts, at a fixed epoch of formation, z_f, with no subsequent star formation at later times, produce a large count excess in the form of a 'hump' in the number counts. If z_f is low (<5), such a hump would lie within the observable range and as such this model is difficult to reconcile with the uniform slope of the counts to very faint magnitudes. If the hump is shifted outside the observable magnitude range by making z_f large, then the *c*-models produce no significant excess of galaxies at intermediate magnitudes. In short, *c*-models with a single epoch of galaxy formation applying to *all* galaxies or the E/S0 subset can be ruled out by the counts alone.

(ii) It is not possible to produce a steep and single-valued count slope for an evolutionary model where one subset of the galaxy population follows a Bruzual μ-model – to be effective in steepening the count slope, the luminosity evolution must be large, and a high redshift tail is expected in $N(z)$. These predictions are listed in Table 5 for comparison with the data (also listed) in terms of the mean redshift, $\bar{z}$, for the magnitude range $20.5 < b_J < 21$ where our data is most complete, and the slope of the differential number magnitude counts, γ, between $20 < b_J < 24$. A count slope marginally consistent with the data can be produced if *all* galaxies follow a 16 Gyr $\mu = 0.5$ model. Models where all galaxies share the same evolutionary history are unphysical, given the observed range in colour for the Hubble sequence, and this model is easily ruled out by the observed redshift distribution, Fig. 3(a).

(iii) If we empirically determine the evolution necessary to fit the counts, in the manner discussed by Shanks *et al.* (1984), we obtain a mean redshift, $\bar{z}$, substantially higher than observed for the μ-model case.

Table 5. Model-predictions and data.

Luminosity Evolution	**Types applied**	$\gamma(20 < b_J < 24)$	$\bar{z}(20.5 < b_J < 21)$
$\mu = .5$ model	E/S0	0.329	0.225
	E/SO-Sbc	0.375	0.246
	ALL	0.419	0.272
Faint Pop. Model		$\gamma(20 < b_J < 24)$	$\bar{z}(20.5 < b_J < 21)$
		0.44	0.17
Steep α Model		$\gamma(20 < b_J < 24)$	$\bar{z}(20.5 < b_J < 21$
$\alpha = -1.50$		0.363	0.183
$\alpha = -1.75$		0.3970	0.148
$\alpha = -2.00$		0.433	0.112
Data		$\gamma(20 < b_J < 23)$	$\bar{z}(20.5 < b_J < 21)$
		0.43±0.02	0.225±0.015

In conclusion, we find that standard models for luminosity evolution cannot simultaneously fit the observed $N(m)$ or $N(z)$. From the counts alone, it appears that there is considerable difficulty in retaining a single slope over such a wide magnitude range, but the determining factor in the absence of a high-redshift tail in our survey which would be expected from the effects of overall-luminosity evolution, whether it be in a subset or in the entire field population observed.

Luminosity evolution in the conventional form discussed in earlier work must therefore have had only a small effect on the photometric properties of galaxies with $z < 0.5$. This suggests that the redshift of galaxy formation is high for any population obeying the c-type models, and that a large proportion of the population might be displaying a fairly constant star-formation rate with look-back time (Tinsley 1980). The major new conclusion from the redshift survey, however, is that at least one extra process needs to be invoked to explain the contrast between the steep slope, γ, of the counts and the unevolved $N(z)$ distribution.

5 The faint end of the luminosity function

5.1 A DWARF-ENRICHED LUMINOSITY FUNCTION?

The luminosity function, determined from bright-field galaxy surveys, is poorly constrained at magnitudes fainter than $M_{b_J} = -17$ (Efstathiou *et al.* 1988, Phillipps & Shanks 1987) because the volumes available for sampling intrinsically faint galaxies in surveys such as DARS (limited at $b_J = 17$) are small and may not contain representative numbers. A larger than expected contribution from such galaxies might explain both the steep count slope and the absence of a high-redshift tail. The steep slope arises naturally because, by virtue of their proximity, such a population would not be subject to redshift dimming and would maintain a Euclidean $10^{0.6}$ mag slope to faint magnitudes. However, to represent a significant change in the count slope, we can expect that a *low redshift* component to $N(z)$ will appear. In this section we examine whether such a model is viable.

The changes in the space density of sub-luminous galaxies required to fit the counts are very large. We find, for example, that if we invoke a new late-type dwarf population whose luminosity function has a standard form ($\alpha = -1.25$, Schechter 1976) but with a characteristic magnitude, $M_J^* = -17.0$, i.e. 4 mag fainter than that of the standard mix, their space density must be 20 times that of the entire bright-galaxy population to reproduce the observed count slope of 0.45 in the range $20 < b_J < 24$. Such a model, whilst extreme, is not significantly ruled out by the observed number of dwarf galaxies sampled to $b_J = 17$.

However, the extremity of this change in the intrinsic properties of the galaxy distribution leads to a major distortion in the predicted redshift distribution, adding a low-redshift component, Fig. 3(a). Table 5 shows that $\bar{z}$ is lowered to ~ 0.17 and is thus clearly incompatible with our redshift distribution.

Alternatively, we can explore the effects of a steeper luminosity slope at the faint end of the luminosity function. Predicted mean redshifts and count slopes for this case are presented in Table 5 for various values of α. A steeper α by itself generates steeper count slopes and lower mean redshifts. For example, if $\alpha = -2$, a significant increase of the count slope is achieved. However, such a value lies well outside the 2σ error ellipse for the DARS survey as a whole, (Efstathiou *et al.* 1988) although conceivably there is still some considerable uncertainty in the actual slope at the faint limit adopted. Note that if one retains the Schechter function shape, adopting a steep luminosity function at the faint end forces the M^*s to be at least 1.0 mag smaller than those adopted in Table 4. This lowers the count slope so that it is *shallower* than our standard no-evolution model ($\gamma = 0.29$).

In conclusion, we find that although the extreme faint end of the luminosity function remains highly uncertain, in terms of Schechter's parameter α, the change required to reproduce the observed steep count slope with a non-evolving model, is unreasonably large. The addition of a dwarf population does provide a viable alternative no-evolution model and whilst one might argue about the precise way in which any dwarf population is incorporated, it is clear that any additional population of local objects invoked to constitute ~ 30 per cent of the galaxies at $b_J \sim 21$, must add a major low-z tail which is ruled out by our redshift distribution.

In fact one can turn the question around and ask what limits our faint survey places on the space density of low-luminosity galaxies in the *field* environment. It is important to recognize that the measuring machines used to construct the photometric galaxy catalogue (on which our survey is based) operates at a threshold of between 25.5 and 26.5 b_J mag arcsec^{-2}, thus dwarfs of exceptionally low surface brightnesses are unlikely to be recognized. None the less, this surface-brightness limit would be sufficient to identify most catalogue dwarfs in the Virgo and Fornax clusters (Phillipps *et al.* 1987). The absence of any galaxies in our survey with $z < 0.03$ is consistent with a luminosity function extrapolated from that determined for bright galaxies; in contrast to the conclusions derived in the Virgo and Fornax clusters.

5.2 EVOLUTION IN THE FAINT END SLOPE

In Section 4 we investigated simple redshift-dependent changes to the luminosity function in an attempt to produce reasonable empirical fits to both the observed $N(m)$ and $N(z)$. Pure luminosity evolution fails to give a satisfactory fit, since the change in magnitude required to reproduce the observed form of $N(m)$ is not consistent with the redshift distribution. In an apparent magnitude-limited survey, greatest weight is given to galaxies with absolute magnitudes close to the characteristic value M^*, and thus the absence of any high-redshift tail is a clear statement that little or no evolution of the bright end of the luminosity function is required.

It is possible, however, to generate a steep $N(m)$ slope without evolving the brightest galaxies, by simply increasing the slope of the faint end of the luminosity function with redshift,

i.e. the only galaxies which we allow to evolve are the precursors of today's intrinsically faint galaxies. This ensures a low mean redshift with respect to pure luminosity evolution, since although the faint end of the luminosity function forms an increasingly important contribution to the *counts* at fainter magnitudes, there is very little change in the bright end. Here we will regard the model as a completely empirical form of *luminosity-dependent* evolution, deferring a discussion of the physical significance until Section 7.

An excellent fit to the data is obtained from the simple relationship that the number of galaxies in any given absolute magnitude bin of 0.02 mag, $N(M)$, evolves over the redshift range $z<1.0$ such that,

$$\log\Phi(M)_z=\log\Phi(M)_{z=0}+(0.1\,z+0.2\,z^2)\log\left[\frac{\Phi(M)}{\Phi(M_0)}\right]_{z=0,}$$

where $\Phi(M_0)_{z=0}=10^{-7}$ Mpc^{-3} 0.02^{-1} mag and $M_0=-23.5$ is the bright end limit of the luminosity function.

Fig. 4 shows the evolution of the luminosity function for the range of observable magnitudes for this case. Note that the low-luminosity limit at a given redshift is determined by the maximum luminosity distance observable for an apparent magnitude limit of $b_J=25.0$.

A count slope of $\gamma=0.43$ for $b_J>20.0$ is obtained in this way, with a mean redshift of $\bar{z}=0.22$ in the range $20.5<b_J<21.0$, in agreement with the data. The resulting redshift distribution is presented in Fig. 3(a). Whilst the range is accurately matched by the data, the distribution is not particularly well-fitted, there being an excess of galaxies observed with $z\sim0.2$. However, examining Fig. 3(b), we can see that this is mostly due to clustering effects within one field (SGP). One expects the *range and mean redshift* of each held to be largely

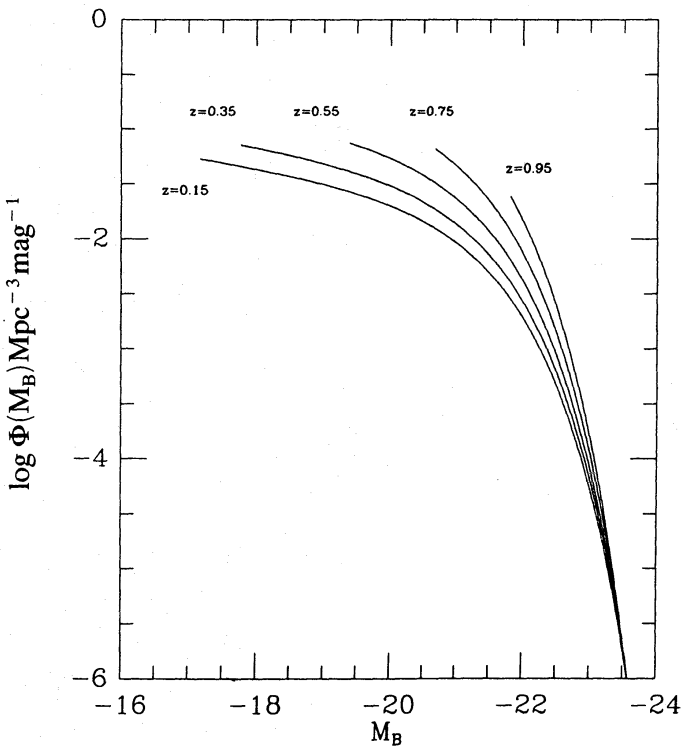

Figure 4. The evolution of the luminosity function described in Section 5.2. This empirical model matches both the observed $N(m)$ and $N(z)$.

insensitive to clustering (as stated earlier) whereas the *distribution* is strongly affected; a comparison of the extreme fields SGP and 197 confirms this behaviour.

6 Spectral evidence for enhanced star formation

The excess counts and bluing trend of galaxies with apparent magnitude have led most reviewers of this subject to infer a higher star-formation rate in galaxies at recent look-back times. As we have discussed, however, this cannot be in the conventional form with accompaning strong-luminosity evolution over the entire luminosity function. In an attempt to understand better what might be responsible for the excess counts, without distorting the redshift distribution, we now examine the spectra of our faint galaxies for evidence of increased star formation.

Conventional star-formation indicators like the Balmer absorption lines or the magnitude of the 4000 Å break, give evidence for recent star formation over a time-period of several Gyr. As such, they are only useful in environments like rich clusters, where there is some homogeneity of the stellar population and where such activity is unusual. With samples dominated by spiral galaxies, where on-going star formation is clearly present, we require an instantaneous indicator of star formation.

We chose the equivalent width of the emission line [O II] 3727 Å as our estimate, for a number of reasons. First, the line is present in over 80 per cent of the sample. Secondly, it is measurable over the entire observed redshift range. Thirdly, as an emission feature which is remarkably strong, it is the only feature at these magnitudes that can be studied with some degree of precision. The major disadvantage of course, is that, unlike Hα, the flux in [O II] cannot directly be linked to the number of hot stars, unless the excitation level is specified. Although, in some cases, this can be checked via the Hβ and [O III]/[O II] line ratios, we will use the [O II] line primarily as an indicator of star-formation *activity* rather than a measure of the star-formation *rate*.

6.1 OBSERVED EQUIVALENT WIDTHS OF [O II] 3727 Å

The rest-frame equivalent width (W_λ) distribution for the new faint survey is shown in Fig. 5. Given the mean sky-subtraction error of 1 per cent averaged over a spectrum, and the continuum level of a galaxy with $20.5 < b_J < 21.5$, the accuracy is typically 5 Å in the rest-frame (Couch & Sharples 1987). We compare this with the same distribution for the local $b_J < 17$ DARS sample. In both cases, the distributions are complete, including objects with no detectable [O II]. Furthermore, we note that those few DARS galaxies with strong [O II] are mostly sub-luminous peculiar spirals. There are very few nearby *luminous* galaxies in this strong-lined category, in marked contrast to the result in the faint survey.

It is immediately apparent from Fig. 5 that objects with strong [O II] are much more numerous in the faint survey. The fraction of galaxies with $W_\lambda > 20$ Å rises from 15 per cent at $b_J < 17$, to 55 per cent at $b_J \sim 21$. However, two important selection effects might in part account for this difference.

First, it is important to consider the physical aperture covered in each survey at their respective mean redshifts. In the case of the faint survey, $\bar{z} \approx 0.21$ and the fibre makes a circular aperture of diameter 2.67 arcsec (12 kpc). For the DARS, $\bar{z} \approx 0.05$ and the slot used to co-add the spectrum had dimensions of 4×20 arcsec (equivalent to 4×21 kpc). Whilst the aperture covers approximately the same area, there is a difference in shape which might bias the faint survey to a greater dominance from disk light and produce the effect seen in Fig. 5. In fact, restricting discussion to the galaxies with strong [O II], we see no correlation between W_λ and

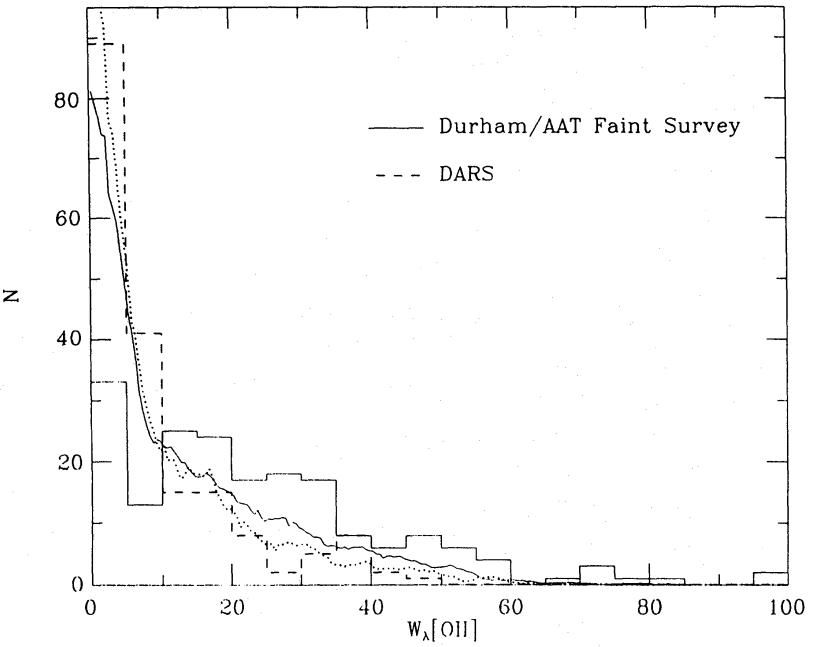

Figure 5. Distribution of rest-frame [O II] 3727 Å equivalent widths for this survey and for the DARS, normalized to the faint survey. Predicted non-evolving equivalent width distributions for DARS and the faint survey are presented as dotted and solid lines, respectively.

redshift *in either sample* as would be expected from this hypothesis in a survey where the distance range is ~ 1 dex. Indeed, the range in equivalent widths for the DARS sample is very similar to that seen in Dressler & Gunn's (1983) local sample of field spirals, where a large circular aperture of diameter 29 kpc was used, whilst that in our faint survey extends to the strongest emission-line galaxies seen in the classical Butcher–Oemler (1978) clusters.

Secondly, the rest-frame wavelength sampled at the mean survey depth of the faint survey is shorter than for the DARS ($\lambda \sim 3700$ *cf.* 4200 Å), and hence the relative difference in k corrections between star forming and quiescent systems will reveal a greater number of the former in the faint survey.

This effect can be quantified for the case of no-evolution, by assuming a correlation between W_λ [O II] 3727 Å and type. For example, by identifying objects of $W_\lambda > 20$ Å as predominantly late types, the no-evolution model predicts that the apparent (detected) ratio of late types to earlier types will only increase by a factor of 1.6 between the bright and faint redshift surveys. The increase observed is, however, far greater, and amounts to a factor of ~ 5 in the proportion of galaxies with $W_\lambda > 20$, ~ 7 for $W_\lambda > 30$.

A more exact calculation can be made by incorporating the observed relation between W_λ [O II] 3727 Å and b_J–K (for the subsample of 109 DARS galaxies with both these measurements), into the b_J–K count model discussed in Section 3.2. As expected, this correlation shows a clear trend to higher equivalent widths for bluer colours. For each colour class of the b_J–K count model, the observed mean equivalent width and scatter are included, and thus we can predict the distribution of W_λ for apparent magnitude-limited samples, assuming no-evolution.

Fig. 5 shows good agreement for distribution of W_λ [O II] 3727 Å in the full sample of DARS with [O II] 3727 Å measurements (191 galaxies), confirming that the subset observed by Mobasher *et al.* (1987) is representative. However, the no-evolution prediction for the faint-redshift survey is not significantly changed; the increase in the ratio of objects predicted to lie

above 20 Å is only 1.8 at $b_J \sim 21$, in agreement with the cruder prediction based on morphological arguments. Thus we conclude that the obvious selection effects resulting from aperture and wavelength coverage differences between this survey and DARS at most account for a small fraction of the difference between the observed equivalent width distributions in Fig. 5.

The fraction of faint-survey galaxies whose W_λ lies in excess of the local distribution approximately matches the count excess at $b_J \sim 21$–21.5 compared with the no-evolution prediction. Since the galaxies with $W_\lambda > 20$ Å are generally the bluest systems, by virtue of their strong star formation, it follows that the same galaxies could be responsible for the small bluing in the colour distribution. Where it is possible to simultaneously measure the [O II], Hβ and [O III] line strengths, the excitation observed is identical to that expected in a star forming H II region (Baldwin *et al.* 1981).

These correlations suggest a straightforward explanation; the excess population seen in the counts can be identified with the star-forming strong emission-line galaxies. This suggestion is borne out by the slope of the counts, $\gamma = d\log N/dm$ examined *as a function of* W_λ for each field and dividing the sample into 0.5 mag bins. We find $\gamma = 0.61 \pm 0.2$ for $W_\lambda > 20$ Å and $\gamma = 0.18 \pm 0.1$ for $W_\lambda < 20$ Å, where the errors are determined from field to field variations. Also, the proportions of objects in these equivalent width ranges are approximately the same, hence the strong line galaxies are clearly making a major contribution to steepening the $N(m)$ slope.

6.2 MODELS FOR EMISSION-LINE GALAXIES

To further clarify the nature of these galaxies we now examine the mean spectrum of this subset (Fig. 6). This spectrum is defined from a subsample of the data for which accurate spectrophotometry on a relative flux scale is possible. A sample of 6 strong emission-line spectra has been selected with a mean $W_\lambda = 40$ Å and range of 35 Å$< W_\lambda <$65 Å. The accuracy of the calibration can be checked by comparing a sample of the reddest spectra with the present-day spectral-energy distribution of a typical elliptical (Pence 1976), assuming the reddest objects at $z \sim 0.25$ are representative of present-day equivalents. Fig. 6(c) shows the agreement between the mean spectrum of five red galaxies observed on a photometric night and Pence's SED is better than ± 5 per cent over the wavelength range of interest.

Clearly, the emission-line galaxies displayed in Fig. 6(a) are undergoing strong star formation. By modelling these spectra under simple assumptions, we can hope to quantify the rate of star formation. We used Bruzual's standard evolutionary synthesis code, improved by Couch & Sharples (1987), to include the intermediate dispersion stellar library of Jacoby, Hunter & Christian (1985). The latter library is perfectly matched in resolution to the data obtained here. Couch & Sharples' models also provide predictions for the emission-line contribution to the spectrum assuming that the recombination spectrum is given by a typical H II region. However, since we are primarly interested in determining the amount of ongoing star formation, we will pay greater regard to matching the Balmer lines and continuum slope, which are more accurately modelled with this code.

First, we examine the degree to which the spectra are indicative of unusually strong star formation, by modelling a system with constant star formation as would be the case for a normal spiral galaxy. We modelled such a galaxy by imposing a constant star-formation rate over 16 Gyr, matching its present day colours to those for typical Sc galaxies and then viewing the galaxy at an age of 10 Gyr. Fig. 6(a) shows the observed spectrum of our star-forming galaxies is quite different, being both bluer and having less prominent Balmer absorption lines. This discrepancy can only be reconciled if galaxies are being observed during a phase when their star-formation rate is much higher than the long-term average.

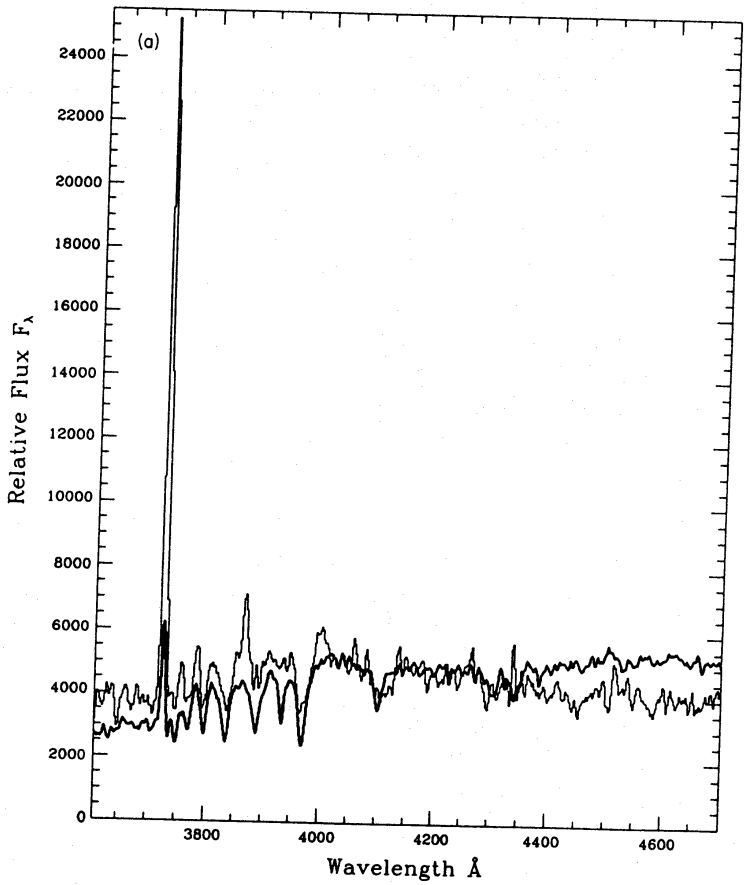

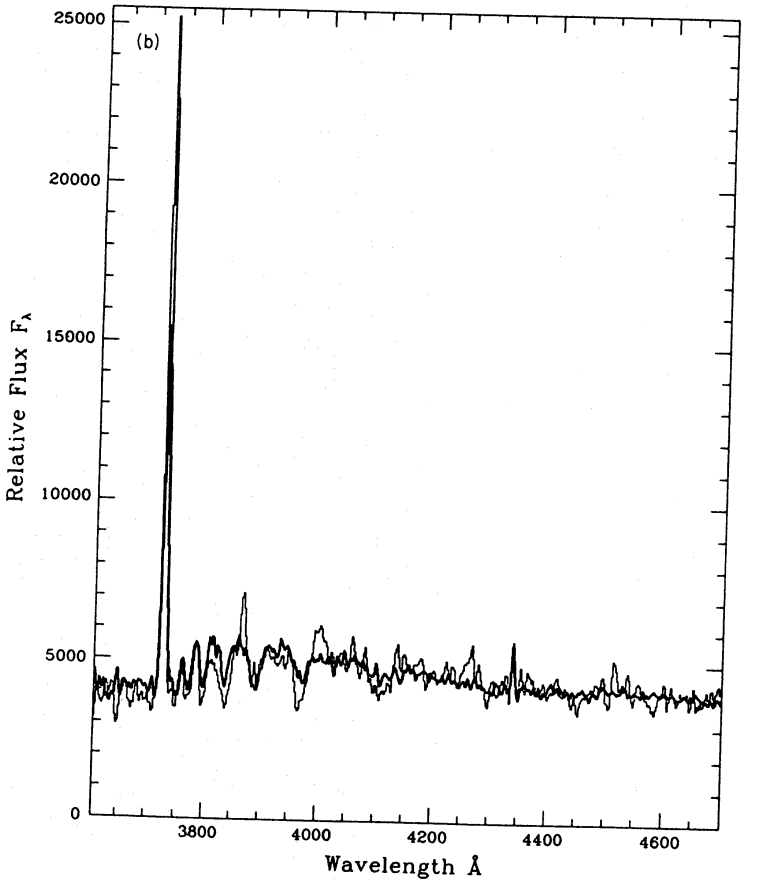

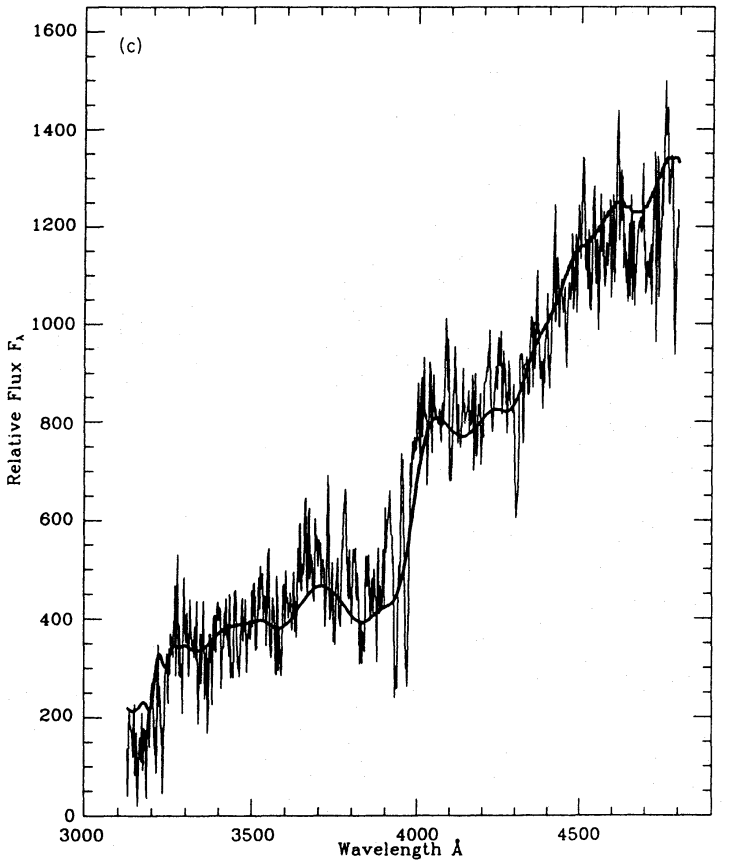

Figure 6. Mean co-added rest-frame spectrum for six survey galaxies wtih $W_\lambda > 35$ Å observed in spectrophotometric conditions. The solid lines are predictions from Bruzual's evolutionary synthesis programme in two cases. (a) Is a model with constant star formation and a gas consumption time-scale of 16 Gyr, viewed 10 Gyr after formation. (b) Is for a galaxy undergoing a second burst of star formation 13 Gyr after formation. The second burst has duration 0.1 Gyr and consumes 5 per cent of the mass of the galaxy. As a spectrophotometric test, (c) is the mean spectrum for five distance galaxies with early-type features compared to their present-day equivalent.

Previous papers by Couch & Sharples (1987), MacLaren, Ellis & Couch (1988) and Ellis (1987b) have described how various spectral features respond to a burst of star formation superimposed on an otherwise quiescent galaxy. If we assume the underlying galaxy underwent a single burst 13 Gyr prior to the observation, then a short secondary burst of duration 0.1 Gyr, converting 5 per cent of the galaxy mass into stars, is sufficient to reproduce the main features observed, Fig. 6(b).

The burst luminosity peaks strongly after 0.1 Gyr and if this burst is viewed at a look-back time of 3 Gyr, which corresponds to the mean redshift of the survey ($z = 0.2$, for $H_0 = 50$, $q_0 = 0.1$), the change in apparent magnitude after 0.1 Gyr is substantial, $\Delta b_J = -2.2$ mag. Since the survey is magnitude-limited, if such bursts are representative, we will preferentially select galaxies at peak burst luminosity. Substantial changes in colour are also expected during such a burst, after 0.1 Gyr at $z = 0.2$ $\Delta(b_J - R_F) = -1.5$ mag, and this may be compared with the shift to bluer colours observed at $b_J \sim 21.5$ (Shanks *et al.* 1984). If residual star formation is present in the underlying spectrum then these changes will be much less extreme. A detailed comparison of burst models and the evolution observed in deep colour distributions is left to a forthcoming paper.

The duration of the burst is restricted by the Balmer lines which would otherwise become too deep. Over the range of masses involved, the result is not very sensitive to the slope of the initial mass function. The brightening implied by a burst of star formation is dependent on the nature of the underlying galaxy; the single burst (c-model) discussed above is the most extreme example. Models show that the effect of a burst of star formation involving a few per cent of the galaxy mass will transform the appearance of the host galaxy, particularly if the time scale is small (Ellis 1987b, Fig. 2), making it very difficult to determine any of the underlying properties.

7 Discussion

Our new redshift survey has shown that if there is a significant evolutionary effect on the photometric properties of galaxies over recent epochs, this can only occur in galaxies that lie today at the faint end of the luminosity function. Whilst the redshift distribution we observe is close to that predicted for no-evolution in the bright end of the luminosity function, we have presented spectral evidence for a general increase with magnitude in the proportion of objects showing enhanced star formation. Modelling shows the enhanced star formation must be shortlived and thus such bursts provide a significant temporary increase in the galaxy luminosity which explains why only a subset of the field population appear to show this evolutionary trend.

The idea that *some* galaxies undergo short bursts of star formation is familiar from spectroscopic studies in distant clusters. This can manifest itself in many ways, of which the most studied example is the blue population in distant concentrated clusters (Butcher & Oemler 1978). Recent detailed spectroscopic (Couch & Sharples 1987; Dressler & Gunn 1983) and photometric (MacLaren *et al.* 1988; Ellis *et al.* 1985) studies have revealed a number of anomalous properties when comparison is made with galaxies in nearby rich clusters. MacLaren *et al.* presented a single unifying hypothesis whereby a galaxy undergoes a short burst of star formation to appear as a blue emission-line galaxy (*cf.* Lavery & Henry 1986). After the star formation ends, the galaxy reveals strong Balmer absorption lines and evidence for the burst can be monitored further via the ultraviolet colours of what are then red galaxies. Constraints on the burst duration and strength from the detailed spectral and colour analysis carried out by these authors indicates that, with a standard initial mass function, 10–30 per cent of the galaxy mass is required to form stars in a period as short as $\sim 5 \times 10^8$ Gyr (Dressler & Gunn 1983). Considering the different environments, the similarity between the burst parameters in clusters and those in the field population (outlined in Section 6.2) is striking.

So far our interpretation of the steepening of the luminosity function with redshift and its connection with the burst model that reproduces the mean spectrum of Fig. 6 has been empirical. In this section we attempt to reproduce the mean redshift, $\bar{z}$, and the slope of the counts, $\gamma = d\log N/dm$ using a physical model that relates the strength of the burst to the mass of the host galaxy. Apart from making our discussion more physical, we wish to explore what further constraints can be made from the observations, e.g. how common the bursting phenomenon has to be, and whether a typical galaxy has undergone a series of events similar to those seen in our survey.

We introduce a dependence of burst strength with galaxy mass by adopting locally determined correlations between star-formation rates, H I content and galaxy luminosity. We invoke simple descriptions of how these relationships may evolve and explore the departures from this model which are required in order to produce a satisfactory fit to the faint distributions. More details of this model will be given in a later paper where we extend the comparison between theory and observations to deeper CCD galaxy counts and colours.

7.1 BURST MODELS

Various workers have shown that the gas content of a galaxy $M_{\mathrm{H\,I}}$ is related to its luminosity, L_g, via a relation of the form

$$L_g \propto (M_{\mathrm{HI}})^{\beta}$$

Observed values of β are greater than 1.0 for late-type systems (Comte 1985), which implies a greater gas mass fraction to B luminosity for lower luminosity galaxies. Unfortunately, similar data for the full range of types is not yet available and uncertainties in this correlation from variations with mass/light ratio suggest that the observations may underestimate the value (Bothun 1984). However, the precise value is not critical for our analysis and in view of these problems we will leave the index β free in the following discussion.

The importance of this expression is that if, as seems reasonable, star-formation rates are proportional to the gas content during a burst, we can now determine the relationship between star formation and galaxy luminosity. To predict observables such as $\bar{z}$ and γ, however, we must integrate the burst models over redshift, taking into account the selection effect that a galaxy undergoing a burst becomes considerably easier to detect. To do this, we calculate the time-dependent rest-frame spectrum of a galaxy of fixed (quiescent) absolute magnitude M_0 undergoing a burst similar to that described in Section 6.2, using Bruzuals' stellar synthesis code for stars formed at a constant rate over 0.1 Gyr. We may then calculate the fractional change in the luminosity of the galaxy ΔM_0 with time, as observed at any redshift, in any passband.

It can be shown that the change in absolute magnitude ΔM at any stage for a galaxy of arbitrary absolute magnitude $M \neq M_0$ is then:

$$\Delta M = 2.5 \log\left[\frac{10^{0.4\Delta M_0}-1}{10^{0.4(1-1/\beta)(M_0-M)}}+1\right].$$

This equation need not relate to the observations referred to above. It can be considered as a more general empirical relationship where the choice of β simply determines the relative dependence of burst luminosity on galaxy luminosity. For example, in the case $\beta = 1.0$, the burst strength is independent of absolute magnitude, whereas a large value of $\beta(>4)$, produces a strong magnitude-dependence for the burst; i.e. evolution is much more important for lower luminosity galaxies.

Since our models deplete the gas with each successive burst (and if star-formation rates are proportional to gas content) there are implications for the relationship between gas content and burst strength. The initial mass function (IMF) adopted for the burst is also important, since its slope and extent determines how much gas is locked up in stars on time-scales longer than those of interest here, and how much can be recycled.

In the simplest case, where a standard Miller & Scalo (1979) IMF is adopted, the gas content is depleted by a fractional amount during each burst, such that the majority of gas consumed is locked up in long lived stars. This results in bursts of successively lower luminosity, and hence an evolutionary picture that is straightforward to calculate. Such a model is strongly constrained by the distribution of local gas contents; the choice of consumed burst gas fraction, f, is determined once the number of bursts, N (in range $0 < z < 1$ say) and the initial burst strength (calculated from ΔM_0) is specified.

Table 6 lists the burst parameters for some cases of this model, with the predictions for the count slope γ and the mean redshift $\bar{z}$ for comparison with Table 5. We make the additional assumption that the bursting population comprises only systems with appreciable gas content, i.e. spiral types, constituting ~ 60 per cent of the total field-galaxy population.

Table 6. Burst model predictions.

$\Delta M_o, M_o$	Gas Fraction	N_1	β	$\gamma(20 < b_J < 24)$	$\bar{z}(20.5 < b_J < 21)$
−1,−19	0.15	18	2.5	0.37	0.27
−1,−19	0.25	12	2.5	0.38	0.24
−1,−19	0.25	12	5	0.40	0.23
−1,−19	0.4	8	5	0.41	0.24
−1,−20	0.25	12	5	0.42	0.28

A steepening of the count slope is produced in this way, with mean redshifts which are lower than those for pure luminosity evolution discussed in Section 4. This model also steepens the luminosity function with redshift which was recognized to be an empirical requirement of the evolution in Section 5.2. However, since this form of evolution is differential ($\beta > 1.0$), our conclusions are somewhat sensitive to the form of the faint end of the luminosity function and the *strength* of this evolution cannot be accurately predicted until the present-day faint population is better understood. For example, a steeper luminosity function today would reduce the amplitude of the evolution required for this type of model, and would thus modify our derived burst strengths and rates.

The point to emphasize, however, is that whatever the precise form of this evolution, it is principally a starburst phenomenon that is producing the steep galaxy–number counts, at least to $b_J \sim 22$. We have placed tight constraints for this form of evolution, combining magnitude and redshift information. More exacting constraints are provided by the addition of deep colour distributions, particularly in the near-ultraviolet, which will be discussed in a subsequent paper.

8 Conclusions

We now summarize conclusions from our statistically complete redshift survey of over 200 galaxies drawn from magnitude-limited samples between $20.0 < b_J < 21.5$.

Our main result is that whilst the slope of the number–magnitude counts at our spectroscopic limiting magnitude argues for an excess of faint blue galaxies, the form of the redshift distribution is in agreement with the no-evolution prediction. This allows us to infer the following.

(i) Luminosity evolution for galaxies at the bright end of the luminosity function must have been very small over the redshift interval $0 < z < 0.5$ and thus such general evolution is not the principle reason why the slope of the blue number magnitude counts is steep at $b_J \sim 21$–23.

(ii) Models invoking a substantial population of intrinsically faint field galaxies are also ruled out by the redshift distribution and cannot provide the count excess.

(ii) The observations are consistent with a simple steepening of the luminosity function with redshift. This may be interpreted as a luminosity dependent luminosity evolution.

(iv) Evidence for strong star formation is found in many of the faint galaxy spectra and good fits to the mean spectrum of this subset can be provided by models incorporating short bursts of star formation. We suggest that the steep slope of the number counts is produced by low luminosity galaxies undergoing such bursts of star formation.

In this largely observational paper, we have concentrated on quantifying the evolutionary effects of the bursts responsible for the spectral features discussed in Section 6. We have not addressed their origin. The similarity between the behaviour of field and cluster galaxies is a

significant clue and it will be important to determine the spatial distribution of the bursting and non-bursting galaxies. Deeper and the more extensive redshift surveys are needed, to realize this aim. In parallel with the new surveys which are beginning, we require detailed modelling of galaxy counts and colours at the faint limits attainable with CCD detectors, to test whether the model we present in Section 7 can account for all the evolution required by the number counts.

Acknowledgments

We thank Peter Gray for his enthusiasm and energy in making the AAT fibre optic coupler a reality; without the multiplex advantage of that instrument this survey would have occupied many hundreds of nights of large-telescope time! We acknowledge invaluable assistance at the telescope from Warrick Couch, and useful discussions with Dick Fong, Jim Gunn, Gus Oemler, David Koo, John Lucey and Ray Sharples. The referee is thanked for many perceptive and challenging remarks. Finally, we acknowledge financial support from the SERC (TJB) and Royal Society (TS).

References

Baldwin, J. A., Phillips, M. M. & Terlevich, R., 1981. *Publs astr. Soc. Pacif.*, **93,** 5.
Bean, A. J., 1983. *PhD thesis,* University of Durham.
Bothun, G. D., 1984. *Astrophys J.*, **277,** 532.
Bruzual, G., 1983. *Astrophys. J.*, **273,** 105.
Butcher, H., Oemler, A., 1978. *Astrophys. J.*, **219,** 18.
Comte, G., 1985. In: *Spectral Evolution of Galaxies,* p. 419, eds Chiosi, C. & Renzini, A., Reidel, Dordrecht.
Couch, W. J. & Sharples, R. M., 1987. *Mon. Not. R. astr. Soc.*, **299,** 423.
Dressler, A. & Gunn, J. E., 1983. *Astrophys. J.*, **263,** 533.
Efstathiou, G. P., Ellis, R. S. & Peterson, B. A., 1988. *Mon. Not. R. astr. Soc.*, **232,** 431.
Ellis, R. S., 1982. In: *The Origin and Evolution of Galaxies,* p. 255, eds Jones, B. J. & Jones, J. E., Reidel, Dordrecht.
Ellis, R. S., 1987a. *Observational Cosmology, IAU Symp. No. 124,* p. 367, eds Hewitt, D. *et al.* Reidel, Dordrecht.
Ellis, R. S., 1987b. *High Redshift and Primeval Galaxies, Third IAP Astrophysics Conference,* p. 3, eds Bergeron, J. *et al.,* Frontieres, Paris.
Ellis, R. S. & Parry, I. R., 1987. *Instrumentation in Astronomy,* Santa Cruz Summer Workshop, p. 192, Springer, Berlin.
Ellis, R. S., Gray, P. M., Carter, D. & Godwin, J., 1984. *Mon. Not. R. astr. Soc.*, **206,** 285.
Ellis, R. S., Couch, W. J., MacLaren, I. & Koo, D., 1985. *Mon. Not. R. astr. Soc.*, **217,** 239.
Gray, P. M., 1986. *Proc. SPIE,* **627,** 96.
Jacoby, G. H., Hunter, D. A. & Christian, C. A., 1984. *Astrophys. J. Suppl.*, **56,** 257.
King, C. R. & Ellis, R. S., 1985. *Astrophys. J.*, **288,** 456.
Koo, D. C., 1981. *PhD thesis,* University of California, Berkeley.
Koo, D. C., 1985. *Astr. J.*, **90,** 418.
Koo, D. C., 1986a. In: *Spectral Evolution of Galaxies,* p. 419, eds Chiosi, C. & Renzini, A. Reidel, Dordrecht.
Koo, D. C., 1986b. *Astrophys. J.*, **311,** 651.
Kron, R. G., 1978. *PhD thesis,* University of California, Berkeley.
Kron, R. G., 1982. *Vistas Astr.*, **26,** 37.
Lavery, R. J. & Henry, J. P., 1986. *Astrophys. J.*, **304,** L5.
Loh, E. D. & Spillar, E., 1986. *Astrophys. J.*, **303,** 154.
MacLaren, I., Ellis, R. S. & Couch, W. J., 1988. *Mon. Not. R. astr. Soc.*, **230,** 249.
Metcalfe, N., Shanks, T., Jones, L. R. & Fong, R., 1987. In: *High Redshift and Primeval Galaxies, 3rd IAP Astrophysics Meeting,* p. 37, eds Bergeron, J. *et al.*, Frontieres, Paris.
Miller, G. E. & Scalo, J. M., 1979. *Astrophys. J. Suppl.*, **41,** 513.
Mobasher, B., Ellis, R. S. & Sharples, R. M., 1987. *Mon. Not. R. astr. Soc.*, **233,** 11.
Morton, D. C., Krug, P. A. & Tritton, K. P., 1985. *Mon Not. R. astr. Soc.*, **212,** 325.
Pence, W. D., 1976. *Astrophys. J.*, **203,** 39.

Peterson, B. A., Ellis, R. S., Kibblewhite, E. J., Bridgeland, M. T., Hooley, T. & Horne, D., 1979. *Astrophys. J.*, **233,** L109.

Peterson, B. A., Ellis, R. S., Bean, A. J., Efstathiou, G., Shanks, T., Fong, R. & Zou, Z.-L., 1986. *Mon. Not. R. astr. Soc.*, **221,** 233.

Phillipps, S. & Shanks, T., 1987. *Mon. Not. R. astr. Soc.*, **227,** 115.

Phillipps, S., Disney, M. J., Kibblewhite, E. J. & Cawson, M. G. M., 1987. *Mon. Not. R. astr. Soc.*, **229,** 505.

Robertson, J. G., 1986. *Publs astr. Soc. Pacif.*, **98,** 1220.

Stevenson, P. R. F., Fong, R., Shanks, T. & Fong, R., 1985. In: *Spectral Evolution of Galaxies,* p. 419. eds Chiosi, C. & Renzini, A. Reidel, Dordrecht.

Schechter, P. L., 1976. *Astrophys. J.*, **203,** 297.

Sharples, R. M., Ellis, R. S., Couch, W. J. & Gray, P. M., 1985. *Mon. Not. R. astr. Soc.*, **212,** 687.

Shanks, T., Stevenson, P. R. F., Fong, R. & MacGillivray, H. T., 1984. *Mon. Not. R. astr. Soc.*, **206,** 767.

Tinsley, B. M., 1980. *Astrophys. J.*, **241,** 41.

Tonry, J. & Davis, M., 1979. *Astr. J.*, **84,** 1511.

Tyson, A., 1987. Preprint.

Tyson, J. A. & Jarvis, J. F., 1979. *Astrophys. J.*, **230,** L153.